Macrophage Impairment Underlies Airway Occlusion in Primary Respiratory Syncytial Virus Bronchiolitis

Jennifer L. Reed,[1]

Yambasu A. Brewah,[1]

Tracy Delaney,[1]

Timothy Welliver,[1,a]

Timothy Burwell,[1]

Ebony Benjamin,[1]

Ellen Kuta,[1]

Alexander Kozhich,[1]

LuAnn McKinney,[1]

JoAnn Suzich,[1]

Peter A. Kiener,[1]

Luis Avendano,[3]

Luis Velozo,[4]

Alison Humbles,[1]

Robert C. Welliver, Sr.,[2] and

Anthony J. Coyle[1]

[1]Respiratory, Inflammation, and Autoimmunity Group, MedImmune, Gaithersburg, Maryland; [2]Department of Pediatrics, Women and Children's Hospital, State University of New York at Buffalo, Buffalo; [3]Programa de Virología, Universidad de Chile, and [4]Departmento de Anatomia Patologica, Roberto del Rio Children's Hospital, Santiago, Chile

Although respiratory syncytial virus (RSV) infection is the most important cause of bronchiolitis in infants, the pathogenesis of RSV disease is poorly described. We studied histopathologic changes in a panel of lung tissue specimens obtained from infants with fatal cases of primary RSV infection. In these tissues, airway occlusion with accumulations of infected, apoptotic cellular debris and serum protein was consistently observed. Similar observations were found after RSV infection in New Zealand black (NZB) mice, which have constitutive deficiencies in macrophage function, but not in BALB/c mice. A deficiency in the number of alveolar macrophages

in NZB mice appears to be central to enhanced disease, because depletion of alveolar macrophages in BALB/c mice before RSV exposure resulted in airway occlusion. In mice with insufficient numbers of macrophages, RSV infection yielded an increased viral load and enhanced expression of type I interferon–associated genes at the height of disease. Together, our data suggest that innate, rather than adaptive, immune responses are critical determinants of the severity of RSV bronchiolitis.

Reprints or correspondence: Dr. Jennifer L. Reed, Food and Drug Administration, Center for Biologics Evaluation and Research, 8800 Rockville Pike HFM-345, Bethesda, MD 20892 (jennifer.reed@fda.hhs.gov).

Respiratory syncytial virus (RSV) infection can result in life‐threatening bronchiolitis and is responsible for ~120,000 hospitalizations of infants in the United States each year [1]. RSV infection in infancy has also been associated with chronic wheezing [2, 3]. The pathogenesis of RSV infection is poorly understood, and most hospitalized infants lack known risk factors [4]. Therefore, further study of the pathogenesis of RSV may improve preventive and therapeutic approaches.

The understanding of RSV pathogenesis primarily has been based on data obtained from experimental models of primary infection in rodents, which generate a robust, T lymphocyte–dominant immune response to RSV [5–6]. Interferon (IFN)–γ production and cytotoxic CD8 T lymphocyte responses limit viral recovery in these models. The development of adaptive responses coincides with airflow limitation, whereas RSV‐associated lung injury is severely blunted in mice lacking both CD4 and CD8 T lymphocytes, despite an increase in virus recovery [7–9]. Thus, T lymphocyte responses in rodents are critical determinants of both RSV clearance and tissue injury. In contrast, the contributions of innate immune responses are less certain. NK cells are thought to promote the antiviral CD8 response, and their recruitment is dependent on binding of RSV F protein (RSV‐F) to Toll‐like receptor (TLR) 4 [10, 11]. However the importance of NK cells either in viral clearance or in the immunopathologic changes associated with RSV has not been established. RSV induces less type I IFN than do other viruses, possibly because of the interfering actions of RSV‐encoded nonstructural proteins [12–15]. Mice lacking the type I IFN receptor (IFNAR) demonstrate virus recovery similar to that shown by wild‐type littermates, with minimal change in lung pathologic findings [15]. Plasmacytoid dendritic cells (pDCs) are an important source of IFN‐α, and studies of pDC depletion have suggested that pDC‐derived IFN‐α limits RSV‐associated tissue injury by suppressing the CD4 T lymphocyte response, rather than through a direct antiviral mechanism [16, 17]. Together, these studies suggest that any role for innate immunity in limiting viral replication is redundant to other clearance mechanisms, and that type I IFN signaling modestly influences immunopathologic changes.

The most serious consequences of RSV infection occur in neonates and elderly individuals, and either immunologic immaturity or an impaired immune response to infection has been implicated in disease exacerbation [18]. In this regard, in vitro studies of alveolar macrophages obtained from infants [19–20] and from elderly subjects [21] have demonstrated multiple functional deficiencies, including impaired

oxidative burst, chemokine release, and phagocytosis, compared with alveolar macrophages acquired from healthy adults. Deficiencies in macrophage function, including poor recognition and uptake of apoptotic cells, have also been reported in patients with systemic lupus erythematosus (SLE) [22, 23] and in multiple mouse strains, including SLE‐predisposed New Zealand mice [24, 25]. Therefore, we investigated the consequences of RSV infection in New Zealand black (NZB) mice, to determine whether impaired macrophage function might affect the respiratory viral disease phenotype. In young NZB mice without the SLE phenotype, we observed greatly enhanced primary RSV disease, with pathologic characteristics strikingly similar to those associated with RSV bronchiolitis in human neonates. Our studies highlight the role of macrophages in both viral clearance and resolution of inflammation associated with RSV infection. In the context of impaired macrophage function, innate immune responses may accelerate immunopathologic changes and provide novel therapeutic targets in serious RSV disease in humans.

Methods

Animals involved in experiments. Six‐week‐old NZB and BALB/c mice were obtained from Harlan and Jackson Laboratories. All in vivo experiments were conducted according to the guidelines of MedImmune's institutional animal care and use committee.

RSV infection. Mice were subjected to anesthesia with isoflurane before intranasal administration of 10^6 pfu of RSV strain A2 (RSVA2). Experiments were terminated on day 6 after infection. For depletion of alveolar macrophages, empty liposomes (NOF Corporation) were formulated with saline buffer with or without clodronate (hereafter referred to as “clodronate liposomes”) (Sigma), according to the manufacturer’s recommendations. Fifty microliters of clodronate liposomes, an equal volume of empty liposomes, or saline vehicle alone was administered intranasally. RSV infection was performed as previously described, 48 h after liposome administration. Anti–mouse IFNAR (provided by R. Schreiber) or isotype control monoclonal antibody (MedImmune) was administered at a dose of 40 mg/kg via the intraperitoneal route, 12 h before infection and then on day 3 after infection.

Virus recovery Lung tissue was homogenized in saline buffer. Serially diluted samples were added to monolayers of Hep2 cells. On day 10 after infection, cell monolayers were fixed and stained with crystal violet to aid in plaque identification. Virus recovery was calculated and expressed as the number of plaque‐forming units per milliliter.

Lung lavage. Animals were euthanized using CO_2. The airway was cannulated and underwent lavage with 0.5 mL of saline. Cytokines and chemokines were measured in lavage fluid by use of commercial kits, and lavage‐associated cells recovered by low‐speed centrifugation underwent flow cytometric analysis for the detection of surface markers. Detailed protocols are provided in appendix A, which is not available in the print version of the *Journal*.

Detection of transcripts and proteins in whole-lung tissue specimens. RNA was purified from whole-lung tissue specimens by use of an RNeasy Plus Mini Kit (Qiagen), and cDNA was synthesized using the Sprint PowerScript Double PrePrimed 96 Kit (Clontech). Gene expression was measured using TaqMan real-time polymerase chain reaction (PCR; Applied Biosystems) performed according to the manufacturer's protocols and is described in appendix A, which is not available in the print version of the *Journal*. For ELISA measurements, lung tissue specimens were homogenized and clarified, and pooled lung tissue specimens were assessed in triplicate wells. Soluble Fas and cytokines were detected using commercial reagents, as detailed in appendix A, which is not available in the print version of the *Journal*.

Macrophage assays. Peritoneal macrophages were collected by lavage with ice-cold saline on day 4 after administration of thioglycollate. Apoptosis was induced in Jurkat cells by treatment with staurosporine, 5 μmol/L, for 24 h. The epithelial cell lines MLE-12 and NZBK (i.e., a respiratory syncytial virus (RSV)–permissive kidney cell line derived from the NZB mouse strain; provided by Jay Levy) were infected with RSVA2 at an MOI of 10 for 24 h. Target cells were labeled with carboxyfluorescein succinimidyl ester (CFSE) and were coincubated with peritoneal macrophages for 45 min. Macrophages were collected, and fluorescence was determined by flow cytometry. To study the release of inflammatory mediators by macrophages, apoptotic cells were opsonized with recombinant galectin-3 (R&D Systems) and then were coincubated with macrophages for 18 h. Cytokines were assessed in supernatants by multiplex ELISA.

Human RSV bronchiolitis. Postmortem lung tissue specimens were obtained from infants with fatal RSV bronchiolitis ($n = 9$) at Hospital Roberto del Rio (Santiago, Chile). RSV infection was confirmed by identification of viral antigen through immunohistochemical analysis (IHCA). Uninfected human lung tissue specimens obtained from infants dying of asphyxia were obtained from the Brain and Tissue Bank for Developmental Disorders at the University of Maryland (Baltimore).

Histopathologic assessment and IHCA. Lungs were inflated with buffered formalin and then were embedded in paraffin blocks for processing. Sections were deparaffinized using consecutive xylene washes, and they were rehydrated using an ethanol gradient. After rehydration, heat-induced epitope retrieval was performed. IHCA was performed using antibodies detecting proliferating cell nuclear antigen (PCNA; AbCam), Fas (Chemicon), or total RSV antigens (Chemicon), according to the manufacturer's instructions.

Statistical analysis. Data are expressed as mean values (±SE). Significance was assessed using a paired Student's *t*-test, with $P < .05$ denoting statistical significance.

Results

Histopathologic characteristics of RSV infection in mice. After inoculation with 10^6 pfu of RSVA2, BALB/c mice develop mild early disease in which virus recovery peaks at approximately day 4 after infection and inflammation peaks at approximately day 6,

when virus recovery is decreasing [5]. At the peak of inflammation, BALB/c mice demonstrate perivascular infiltration and interstitial accumulation of lymphocytes; there is no occluding material in the airway, and peribronchiolar inflammation is sparse (figure 1*A–C*). We expected to find similar characteristics of acute infection in 6-week-old NZB mice, which have the same H-2d haplotype as BALB/c mice and display no autoimmune symptoms. Instead, we found greatly enhanced acute respiratory disease that was fatal in ~30% of NZB mice by day 6 after infection. Histologic assessment of lung tissue specimens demonstrated a massive immune cell infiltrate around vessels and bronchioles and within alveolar spaces (figure 1*D–F*). Occlusion of small and large airways with an admixture of serum protein, cellular debris, and inflammatory cells was prominent (figure 1*E*, *arrowheads*). The obstructing material and bronchiolar epithelium were found to have negative results of periodic acid–Schiff (PAS) staining (figure 1*F*). Enhanced disease in NZB mice was entirely dependent on virus infection, because UV-irradiated virus yielded no inflammation or airway occlusion (see figure B1, in appendix B, which is not available in the print version of the *Journal*).

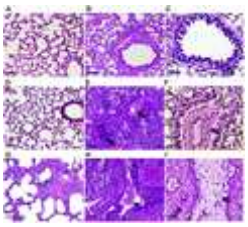

Figure 1. Histopathologic assessment of respiratory syncytial virus (RSV) infection in mouse and human lung tissue. Five- to 6-week-old BALB/c *(A–C)* and New Zealand black (NZB) *(D–F)* mice were inoculated with 10^5 pfu of RSV strain A2 via the intranasal route. Lung tissue specimens were collected on day 6 after infection. Hematoxylin-eosin (HE) staining and periodic acid–Schiff (PAS) staining were performed on formalin-fixed tissue sections. *A*, and *D*, HE-stained tissue from uninfected mice; HE-stained tissue (*B* and *E*) and PAS-stained tissue (*C* and *F*) specimens obtained from RSV-infected mice on day 6 after infection. *G*, Uninfected pediatric lung tissue specimens stained with HE. RSV bronchiolitis–affected lung tissue specimens, stained with HE *(H)* or PAS stain *(I)*. Arrows denote airway occlusions. The bar denotes 30 μm (except for PAS stains [*C*, *F*, and *I*], for which the bar denotes 15 μm).

Comparison with RSV disease in human neonates. Histologically, the pathologic changes observed in NZB mice after RSV infection were strikingly similar to the changes recently observed in humans neonates with RSV disease [26]. Analysis of tissue specimens obtained at autopsy from human neonates with RSV bronchiolitis revealed dense inflammatory infiltrate and occlusion of the airway with PAS-negative serum protein and fluid mixed with cellular debris (figure 1*G–I*). In lung tissue specimens obtained from both RSV-infected NZB mice and from humans with fatal RSV bronchiolitis, RSV antigen was prominently detected in both the alveolar and the bronchiolar epithelium, as well as in the cellular debris within occlusions (figure 2). In addition, robust expression of the apoptosis marker Fas (figure 3*A*) and the proliferation marker PCNA (figure 3*B*) was detected in the respiratory epithelium, suggesting ongoing epithelial apoptosis and reparative processes in both humans and NZB mice after infection. Enhanced Fas expression in the susceptible NZB strain at the peak of

RSV infection was confirmed by ELISA performed on whole-lung homogenates (see table C1, in appendix C, which is not available in the print version of the *Journal*).

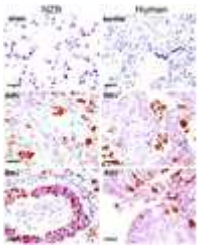

Figure 2. Respiratory syncytial virus (RSV) antigen detection in New Zealand black (NZB) mice after RSV infection and in humans with RSV bronchiolitis. Detection of RSV antigens by immunohistochemical analysis (IHCA) of lung tissue obtained from NZB mice before and after RSV infection *(left panels)* and of uninfected lung tissue and RSV bronchiolitis–affected tissue obtained at autopsy from human infants *(right panels).* RSV-positive alveolar tissue specimens *(middle panels)* and RSV-positive bronchiolar epithelium *(bottom panels)* are shown. The bar denotes 15 μm.

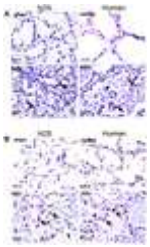

Figure 3. Epithelial activation in New Zealand black (NZB) mice after respiratory syncytial virus (RSV) infection and in humans with RSV bronchiolitis. Detection of *(A)* Fas and *(B)* proliferating cell nuclear antigen by immunohistochemical analysis (IHCA) of lung tissue specimens obtained from NZB mice before and after RSV infection *(left)* and of uninfected lung tissue and RSV bronchiolitis–affected tissue specimens obtained from human infants at autopsy *(right).* IHCA was performed on formalin-fixed, paraffin-embedded lung tissue specimens by use of an antigen-retrieval method. Arrowheads denote alveolar epithelial cells. The bar denotes 15 μm.

Antiviral cytotoxic responses in mice. Recovery of virus from susceptible NZB mice was increased 10-fold, compared with recovery from BALB/c controls (see table C1, in appendix C, which is not available in the print version of the *Journal*). Therefore, we investigated whether an inefficient or skewed immune response to RSV might be responsible for both increased viral recovery and greater lung tissue damage. Previous studies involving immunocompetent mouse models have implicated irregularities of the adaptive immune response, either lymphocyte hypersensitivity or altered T helper lymphocyte skewing, in enhanced acute RSV disease and delayed viral clearance [5–9, 16, 17]. We recovered fewer T lymphocytes from the lungs of NZB mice, compared with BALB/c mice (figure 4*A*), with similar CD4:CD8 ratios and similar IFN-γ production noted in the 2 strains. Thus, enhanced T lymphocyte responses to virus infection seemed not to be responsible for enhanced disease in NZB mice. We also examined whether CD8 T cells were functionally flawed in the NZB strain. In a flow cytometry–based assay, lung lymphocytes exhibited cytolytic activity against an RSV-infected, major histocompatibility complex (MHC)–matched epithelial cell line.

The cytolytic activity of lymphocytes acquired from NZB mice was similar, on a per‐cell basis, to that of lymphocytes acquired from the BALB/c strain (see figure B2, in appendix B, which is not available in the print version of the *Journal*). In summary, we observed an ~4‐fold reduction in $CD8^+$ T cells in susceptible NZB mice, compared with MHC‐matched BALB/c mice, with normal IFN‐γ production and no intrinsic defect in cytolytic activity noted. Taken together, these subtle differences in adaptive immunity are insufficient to explain the extreme susceptibility of NZB mice to RSV.

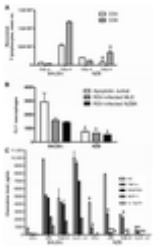

Figure 4. Lymphocyte and macrophage responses to respiratory syncytial virus (RSV) infection. *A*, Lung‐associated lymphocytes after RSV infection. BALB/c and New Zealand black (NZB) ($n = 5$) mice were inoculated with 10^6 pfu of RSV strain A2. Immune cells recovered by lung lavage were analyzed by flow cytometry for the presence of CD4 ($CD3^+CD8^-CD49b^-$) and CD8 ($CD3^+CD8^+CD49b^-$) lymphocytes. The mean no. of recovered lymphocytes (±SE) is shown. Data representative of 3 experiments are shown. *B*, Macrophage uptake of apoptotic T lymphocyte and RSV‐infected epithelial target cells. Thioglycollate‐elicited peritoneal macrophages were incubated with carboxyfluorescein succinimidyl ester (CFSE)–labeled targets. The mean no. of CFSE‐positive macrophages (±SE) recovered from 4 wells is shown. Data representative of 3 experiments are shown. *C*, Release of inflammatory mediators. Peritoneal macrophages were challenged ex vivo for 18 h with opsonized (opson.) apoptotic lymphocytes or RSV‐infected epithelial cells. Released inflammatory mediators were measured by multiplex ELISA performed in triplicate. Mean ± SE are reported. Data representative of 3 experiments are shown. IL‐12p70, interleukin‐12 40‐kDa subunit; KC, keratinocyte‐derived chemokine; MCP‐1, monocyte chemotactic protein–1; MLE, mouse lung epithelial cell line, derived from the FVB mouse strain (permissive for RSV infection); NZBK, a RSV–permissive kidney cell line derived from the NZB mouse strain; Poly I:C, polyinosinic:polycytidylic acid; RANTES, regulated on activation, normally T cell expressed and secreted; TNF, tumor necrosis factor. *$P \leq .05$; **$P \leq .01$.

Antiviral and anti‐inflammatory macrophage functions in mice. Mice prone to autoimmune disease, including New Zealand strains, have deficiencies in macrophage function, including poor recognition and phagocytosis of apoptotic cells [24, 25]. We tested macrophages obtained from BALB/c and NZB mouse strains for the uptake of 3 separate cellular targets: RSV‐infected mouse epithelial cells derived from either NZB or FVB strains and from apoptotic Jurkat T lymphocytes. NZB macrophages were less efficient at target cell uptake (figure 4*B*). To determine whether the release of inflammatory mediators from macrophages differed between NZB and BALB/c mice, macrophages were stimulated with nonspecific stimuli, such as Toll receptor ligands or opsonized target cells, for 18 h, and supernatants were analyzed for proinflammatory mediators. Activated BALB/c macrophages released high quantities of chemokines, including keratinocyte‐derived chemokine (KC); regulated on activation, normally T

cell expressed and secreted (RANTES); monocyte chemotactic protein–1 (MCP□1); and tumor necrosis factor (TNF)–α (figure 4*C*). BALB/c macrophages also secreted interleukin (IL)–12 70□kDa subunit (IL□12p70) after TLR4 ligand stimulation.

In contrast, after stimulation with Toll ligands or opsonized cell targets, NZB macrophages produced less KC and TNF□α, little MCP□1, and no IL□12 p70 with lipopolysaccharide stimulation. We hypothesized that the hyporesponsiveness of macrophages to RSV□infected targets and apoptotic inflammatory cells might be associated with bronchiolar occlusion, and we considered the possible role of alveolar macrophages in limiting RSV□associated disease in BALB/c mice. In published studies of clodronate liposome formulations [27], a single intranasal administration depleted alveolar macrophages from the lungs of healthy BALB/c mice within 48 h, without triggering recruitment of inflammatory cells to the tissue. We confirmed this observation in our own studies (see figure B3, in appendix B, which is not available in the print version of the *Journal*). We therefore compared primary RSV infection in BALB/c mice that received an intranasal dose of clodronate liposomes with primary RSV infection in BALB/c mice that received saline vehicle control. We also examined RSV infection in mice receiving empty liposomes, which dampen the phagocytic capacity of macrophages without cell depletion [28]. Recovery of virus from the lungs was increased >10□fold in animals receiving either clodronate liposomes or empty liposomes before RSV infection, compared with animals receiving saline vehicle (figure 5*A*). Overall, inflammation was similar among all RSV□infected groups. However, bronchiolar occlusion with serum protein and cellular debris was present in BALB/c mice receiving the empty liposome formulation, and it was prominent in BALB/c mice with alveolar macrophage depletion (figure 5*B–C*). Of note, inflammatory mediators associated with macrophage activation in vitro, including RANTES, KC, TNF□α, and macrophage inflammatory protein–1α (MIP□1α), were reduced in the lung tissue of clodronate liposome recipients after RSV infection (see table C2, in appendix C, which is not available in the print version of the *Journal*). IFN□γ levels were elevated after RSV infection in all treatment groups and did not correlate with blockade of the airways.

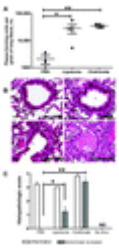

Figure 5. Depletion of alveolar macrophages before respiratory syncytial virus (RSV) infection in BALB/c mice. BALB/c mice received saline (PBS), empty liposomes (Liposome), or liposomes formulated with clodronate (Clodronate) via the intranasal route before inoculation with 10^5 pfu of RSV strain A2. *A*, On day 4 after infection, whole□lung tissue specimens were harvested from a subset of mice. Virus recovery was assessed by plaque assay from tissue homogenates. *B*, Hematoxylin□eosin staining of formalin□fixed tissue sections was performed on day 6 after infection. Representative bronchioles from each group are shown. The arrow denotes airway occlusion. *C*, Histopathologic findings associated with RSV infection were evaluated (5 mice/group). Overall inflammation *(gray bars)* and bronchiolar occlusion *(white bars)* were

separately assessed. Mean values (±SE) are shown. ND, no inflammation and occlusion detected. *$P \leq .05$; **$P \leq .01$.

Innate antiviral mechanisms in mice. Inefficient macrophage responses in NZB mice appeared to be associated with an elevated viral load and more severe RSV-associated disease. Because abnormalities in innate immune function have been observed in the NZB strain [29], we considered whether dysregulation of additional innate antiviral mechanisms might contribute to enhanced RSV disease. We first studied NK cells, which are thought to limit RSV infection through lysis of virus-infected targets and local secretion of IFN-γ [10]. We observed greatly expanded numbers of NK cells in the lungs of susceptible NZB mice after RSV infection, compared with BALB/c control mice (figure 6*A*), a finding that suggests that NK cells were functional and their activity perhaps exaggerated after infection in NZB mice. Next, we examined type I IFN signaling, which is associated with the intracellular antiviral state (reviewed in [30]), and pDCs, which are thought to amplify the antiviral state by providing a burst of cytokines, including IFN-α and TNF–α [16, 17]. $Gr1^+CD11c^+$ pDCs were greatly enhanced in the lung tissue of NZB mice after RSV infection (figure 6*B*). Although neither IFN-α nor IFN-β was detected in lung tissue specimens by use of ELISA (data not shown), there was an ~30-fold increase in the type I IFN–induced transcript oligoadenylate synthetase 3 (OAS3), the IFN-induced gene with tetratricopeptide repeat 1 (IFIT1), and IFN-induced gene 44 (IFI44), at the peak of illness in NZB mice, compared with sham-infected mice (figure 6*C*). Monokine induced by IFN-γ (MIG) protein was increased in the lungs of NZB mice after RSV infection (see table C1, in appendix C, which is not available in the print version of the *Journal*). In addition, after infection, IFN-inducible myxovirus resistance (Mx) protein was robustly detected in the bronchiolar epithelium, where viral antigen was localized (see figure B4, in appendix B, which is not available in the print version of the *Journal*).

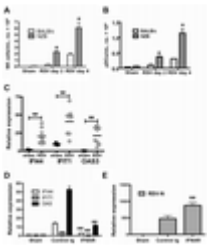

Figure 6. Type I interferon (IFN) signaling pathways in New Zealand black (NZB) mice after respiratory syncytial virus (RSV) infection. Mice were inoculated with 10^5 pfu of RSV strain A2. On days 2 and 4 after infection, the animals were euthanized, and lung tissue underwent lavage with saline. Recovered NK cells ($CD49b^+CD3^-$) *(A)* and plasmacytoid dendritic cells (pDCs) ($CD11c^+Gr1.1^+$) *(B)* were assessed by flow cytometry. The mean no. of cells (±SE) recovered from 5 mice is shown. Data representative of 3 experiments are shown. *C,* Total RNA was recovered from the lung tissue of NZB mice ($n = 7$) that were inoculated with RSV or with vehicle control (i.e., sham inoculated). IFN-inducible genes were assessed using quantitative polymerase chain reaction (qPCR) on day 6 after infection. IFN-inducible genes *(D)* and RSV N protein (RSV-N) transcript *(E)* were assessed on day 6 after infection in NZB mice ($n = 7$) that were sham inoculated (sham) or that received a type I IFN receptor (IFNAR) neutralizing antibody or irrelevant isotype control antibody (control Ig), before infection. OAS, type I IFN–induced transcript oligoadenylate synthetase 3;

IFIT1, IFN-induced gene with tetratricopeptide repeat 1; IFI44, IFN-induced gene 44. *$P \leq .05$; **$P \leq .01$.

Similar codetection of Mx protein with viral antigen was found in BALB/c mice in which alveolar macrophages were depleted before RSV infection, but not in BALB/c mice with intact lung macrophages (see figure B5, in appendix B, which is not available in the print version of the *Journal*). We then considered whether defects in the intracellular antiviral state might contribute to enhanced viral burden in NZB mice. To address this hypothesis, NZB mice were administered a prophylactic dose of IFNAR neutralizing monoclonal antibody or an isotype-matched control antibody before RSV infection. The IFNAR neutralizing antibody significantly reduced detection of IFIT1, OAS3, and IFI44 (figure 6*D*). At the same time, detection of the RSV transcript encoding N protein was enhanced (figure 6*E*), suggesting that the intracellular antiviral state was functional in infected NZB mice. Thus, innate immune pathways appear to be intact, exaggerated, and yet insufficient to clear RSV infection in NZB mice.

Discussion

In immunocompetent mouse models, and, presumably, in adult humans who have limited lung pathologic findings after RSV infection, cytotoxic and IFN-γ–producing lymphocytes, including NK cells and $CD8^+$ T cells, contribute to protection by limiting virus replication and destroying virus-infected epithelial cells. Depletion of $CD8^+$ and $CD4^+$ lymphocytes in immunocompetent mice results in higher virus recovery after infection, but it does not lead to the extensive inflammation and obstruction of the airway lumen seen in NZB mice in this study [9]. This observation points to a second mechanism (not requiring lymphocytes) that limits inflammation after primary RSV infection. Our data strongly suggest that the alveolar macrophage is responsible for attenuating lung inflammation triggered by RSV. In NZB mice, which lack normal macrophage responses to infected cells and apoptotic debris, enhanced RSV immunopathologic findings were observed. In fact, numbers of cytolytic NK and CD8 cells, together with the level of local IFN-γ secretion, were in the range considered to be normal in NZB mice and yet were not sufficient to limit acute RSV disease. Similar enhanced disease was observed in wild-type BALB/c mice in which alveolar macrophage function was antagonized using either clodronate liposomes to deplete macrophages outright or empty liposomes to saturate phagocytic capacity without depletion. It is important to note that, even in immunocompetent animals, NK cells and CD8 lymphocytes, which are minimally phagocytic cells [31], and IFNs do not clear virus by themselves but, instead, facilitate destruction of infected cells in a process that is completed by phagocytic macrophages. This paradigm has been demonstrated in mouse models of vesicular stomatitis virus and lymphocytic choriomeningitis virus infection, in which depletion of a subset of splenic macrophages yielded enhanced virus recovery with increased morbidity and mortality, despite high levels of IFN and the presence of both Th1 and Th2 adaptive antiviral immune responses [32–34].

Apoptotic cellular debris, if left uncleared by macrophages, is injurious. In models of acute lung injury, IFN-β elaborated from injured cells induces bystander apoptosis and recruits granulocytes [34–36]. Persistent debris also further antagonizes macrophage

function, a process implicated in the “vicious circle” of SLE pathogenesis [37]. In BALB/c mice and NZB mice with alveolar macrophage depletion, we propose that reduced macrophage function delays clearance of virions and infected epithelial cells (figure 7, *left panels*). The hyporesponsiveness of macrophages in the lung boosts virus replication and cell‐to‐cell spread (figure 7, *left middle panel*). Type I IFN and other chemokines expressed by infected epithelia recruit immune cells, which undergo apoptosis after activation in lung tissue. These late apoptotic cell corpses, left uncleared by macrophages (figure 7, *bottom left*), release such factors as IFN‐β, MIG, and IFN‐γ–inducible protein–10 (IP‐10), which recruit additional inflammatory cells and accelerate tissue destruction. Thus, acute, enhanced RSV disease in macrophage‐insufficient mice (and, perhaps, in human infants) results from both a failure to clear virus‐infected cells and a failure to limit inflammation and bystander injury [38, 39]. Similar conclusions were reached in a recent study of parainfluenza virus infection in RANTES‐deficient mice, in which viral persistence, enhanced inflammatory cell infiltration, and increased mortality were observed [40]. In that study, RANTES appeared to be critical in maintaining lung macrophage survival in the face of viral infection and, therefore, bolstered virus clearance. In our models, expression of RANTES after RSV infection was limited both in NZB mice and in BALB/c mice with alveolar macrophage depletion, perhaps suggesting an autocrine/paracrine role for RANTES in maintaining alveolar macrophage survival or function after viral challenge.

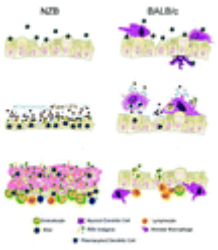

Figure 7. Comparison of respiratory syncytial virus (RSV)–associated pathologic findings in New Zealand black (NZB) and BALB/c mouse strains. In NZB mice, a deficient uptake of input virions by alveolar macrophages results in unchecked epithelial infection *(top left).* Inflammatory mediators, especially type I IFN, are released from infected and apoptotic cells *(middle left).* Failure of NZB macrophages to clear epithelial cell corpses *(lower left)* results in occlusion of the airway lumen and bronchiolitis. In BALB/c mice, alveolar macrophages and dendritic cells intercept input virions *(top right),* limiting epithelial infection. Continued macrophage surveillance of the epithelium results in rapid removal of infected cells and apoptotic debris from the airway *(middle right).* The peak of RSV disease in BALB/c is characterized by lymphocyte recruitment *(lower right)* in response to a decreasing RSV burden, with minimal epithelial involvement.

These observations underscore the role of lung macrophages as sentinels in lung tissue (figure 7, *right panels*). In addition to scavenging virions and infected cells, macrophages are an early source of chemokines after infection (figure 7, *middle right panel*). This early chemokine burst rapidly recruits cytotoxic and IFN‐γ–secreting lymphocytes, curtailing the spread of virus in the lung epithelium (figure 7, *bottom right panel*). The highly efficient macrophage response to RSV in rodent strains typically used for animal models possibly explains the requirement for extremely high inocula to induce disease in these animals [5, 6]. Moreover, the pathologic changes induced in

these high‐inoculum models appear to represent hyperactivation of an otherwise appropriate response to virus in animals with normally functioning macrophages.

The similarity between RSV‐induced damage in NZB mice and human infants suggests a common pathogenesis. The immunologic function of lung macrophages in human neonates is incompletely studied; however, maturational defects in infant alveolar macrophages, cord blood macrophages, and monocytes [19–20, 41–43] have been reported. Previous studies of monkeys [44], rats [45], and rabbits [46, 47] have also demonstrated functional immaturity of alveolar macrophages during neonatal life. Genetic conditions that impair pulmonary macrophage function also have been associated with an increased risk of severe RSV disease [48–50]. On the basis of these findings, it seems quite possible that uptake of infected epithelial cells, recruited immune cells, and damaged bystanders by alveolar macrophages is inefficient in infants, as in NZB mice, and may be the shared basis for predisposition to severe RSV disease. Vaccination strategies with the potential to stimulate local macrophage function safely may be particularly effective approaches in infants and others with compromised lung macrophage function.

In response to RSV, human neonates and NZB mice displayed apoptotic airway epithelial cells, reparative epithelial processes, and occlusion of airways with mucin‐poor material. Importantly, these pathologic changes are in marked contrast to those associated with other respiratory conditions featuring airway occlusion. For example, in human allergic asthma and rodent models of asthma, Th2 lymphocytes and their associated cytokines are critical contributors to disease; moreover, there is little to no activation of type II alveolar cells, and the airway lumen is occluded with PAS‐positive mucus produced by proliferative bronchiolar epithelia. These observations demonstrate that at least 2 distinct pathologic processes can lead to airway occlusion. These 2 pathways may differentially contribute to bronchiolitis, asthma, or asthma exacerbated by respiratory virus infection. A more complete understanding of the inflammatory cascade associated with persistent apoptotic debris may yield novel strategies in the treatment of respiratory diseases featuring airway occlusion.

Acknowledgments

We thank Jay Levy for providing New Zealand black–derived kidney epithelial cells; Donna Goldsteen and Nanci Donacki for their excellent technical help; and Gary Sims, Ricardo Cibotti, Ari Theofilopoulos, and Richard Spaete for helpful discussion.

Supplementary Materials and Methods

Antibodies for ELISA and flow cytometry. Cytokine and chemokine levels were measured in lavage fluid by use of commercial kits from Linco, for cytokine detection by Luminex multiplex assay, and from R&D Systems, for standard ELISA detection of interferon (IFN)–γ, interleukin‐10, and monokine induced by IFN‐γ. For flow

cytometric analysis, antibodies recognizing Gr1, Ly49, CD11c, CD11b, CD3, CD4, and CD8 were obtained from Becton Dickinson Biosciences. Soluble Fas was detected in mouse lung homogenates by use of a commercially available ELISA kit (R&D Systems). Cytokine mediators were measured using a commercial multiplex kit (Linco).

RNA extraction and real□time quantitative polymerase chain reaction (PCR) analysis. After purification of RNA with an RNeasy Plus Mini Kit (Qiagen), cDNA was synthesized using a Sprint PowerScript Double PrePrimed 96 Kit (Clontech). Gene expression was measured using TaqMan real□time PCR (Applied Biosystems) according to the manufacturer's protocols. The probe sets were obtained from Applied Biosystems as TaqMan gene expression assays. PCRs contained either the reference gene (glyceraldehyde 3□phosphate dehydrogenase) or the genes of interest: IFN□induced gene 44, IFN□induced gene with tetratricopeptide repeat 1, type I IFN–induced transcript oligoadenylate synthetase 3, and RSV N protein. The experiments were performed using an ABI Prism 7700 Sequence Detection System (Applied Biosystems) under the following conditions: 2 min at 50°C and 10 min at 95°C, followed by 2□step PCR performed for 40 cycles for 15 s at 95°C, followed by 1 min at 60°C. The number of PCR cycles needed to cross a threshold of a statistically significant increase in fluorescence (with "Ct" denoting the threshold cycle) was measured using Applied Biosystems software.

Supplementary Figures

Jump To Section...

Supplementary Tables

Jump To Section...

References

Jump To Section...

- 1. Paramore LC, Ciuryla V, Ciesla G, Liu L. Economic impact of respiratory syncytial virus□related illness in the US: an analysis of national databases. Pharmacoeconomics **2004**; 22:275–84.

- 2. Sigurs N, Gustafsson PM, Bjarnason R, et al. Severe respiratory syncytial virus bronchiolitis in infancy and asthma and allergy at age 13. Am J Respir Crit Care Med **2005**; 171:137–41.

- 3. Bradley JP, Bacharier LB, Bonfiglio J, et al. Severity of respiratory syncytial virus bronchiolitis is affected by cigarette smoke exposure and atopy. Pediatrics **2005**; 115:e7–14.

- 4. La Via WV, Grant SW, Stutman HR, Marks MI. Clinical profile of pediatric patients hospitalized with respiratory syncytial virus infection. Clin Pediatr **1993**; 32:450–4.

- 5. Domachowske JB, Bonville CA, Rosenberg HR. Animal models for studying respiratory syncytial virus infection and its long term effects on lung function. Pediatr Infect Dis J **2004**; 23:S228–34.

- 6. Peebles RS, Graham BS. Pathogenesis of respiratory syncytial virus infection in the murine model. Proc Am Thoracic Soc **2005**; 2:110–5.

- 7. van Schaik SM, Obot N, Enhorning G, et al. Role of interferon gamma in the pathogenesis of primary respiratory syncytial virus infection in BALB/c mice. J Med Virol **2000**; 62:257–66.

- 8. Alwan WH, Record FM, Openshaw PJ. $CD4^+$ T cells clear virus but augment disease in mice infected with respiratory syncytial virus: comparison with the effects of $CD8^+$ T cells. Clin Exp Immunol **1992**; 88:527–36.

- 9. Graham BS, Bunton LA,Wright PF, Karzon DT. Role of T lymphocyte subsets in the pathogenesis of primary infection and rechallenge with respiratory syncytial virus in mice. J Clin Invest **1991**; 88:1026–33.

- 10. Hussell T, Openshaw PJ. Intracellular IFN□gamma expression in natural killer cells precedes lung $CD8^+$ T cell recruitment during respiratory syncytial virus infection. J Gen Virol **1998**; 79:2593–601.

- 11. Haynes LM, Moore DD, Kurt□Jones EA, Finberg RW, Anderson LJ, Tripp RA. Involvement of Toll□like receptor 4 in innate immunity to respiratory syncytial virus. J Virol **2001**; 75:10730–7.

- 12. Spann KM, Tran KC, Chi B, Rabin RL, Collins PL. Suppression of the induction of alpha, beta, and lambda interferons by the NS1 and NS2 proteins of human respiratory syncytial virus in human epithelial cells and macrophages. J Virol **2004**; 78:4363–9.

- 13. Lo MS, Brazas RM, Holtzman MJ. Respiratory syncytial virus nonstructural proteins NS1 and NS2 mediate inhibition of Stat2 expression and alpha/beta interferon responsiveness. J Virol **2005**; 79:9315–9.

- 14. Ramaswamy M, Shi L, Varga SM, Barik S, Behlke MA, Look DC. Respiratory syncytial virus nonstructural protein 2 specifically inhibits type I interferon signal transduction. Virol **2006**; 344:328–39.

- 15. Johnson TR, Mertz SE, Gitiban N, et al. Role for innate IFNs in determining respiratory syncytial virus immunopathology. J Immunol **2005**; 174:7234–41.

- 16. Smit JJ, Rudd BD, Lukacs NW. Plasmacytoid dendritic cells inhibit pulmonary immunopathology and promote clearance of respiratory syncytial virus. J Exp Med **2006**; 203:1153–9.

- 17. Wang H, Peters N, Schwarze J. Plamsacytoid dendritic cells limit viral replication, pulmonary inflammation, and airway hyperresponsiveness in respiratory syncytial virus infection. J Immunol **2006**; 177:6263–70.

- 18. van Drunen Littel–van den Hurk S, Mapletoft JW, Arsic N, Kovacs□Nolan J. Immunopathology of RSV infection: prospects for developing vaccines without this complication. Rev Med Virol **2007**; 17:5–34.

- 19. Grigg J, Riedler J, Robertson CF, Boyle W, Uren S. Alveolar macrophage immaturity in infants and young children. Eur Respir J **1999**; 14:1198–205.

- 20. D'Ambola JB, Sherman MP, Tashkin DP, Gong H Jr. Human and rabbit newborn lung macrophages have reduced anti□*Candida* activity. Pediatr Res **1988**; 24:285–90.

- 21. Plowden J, Renshaw□Hoelscher M, Engleman C, Katz J, Sambhara S. Innate immunity in aging: impact on macrophage function. Aging Cell **2004**; 3:161–7.

- 22. Gaipl US, Voll RE, Sheriff A, Franz S, Kalden JR, Herrmann M. Impaired clearance of dying cells in systemic lupus erythematosus. Autoimmun Rev **2005**; 4:189–94.

- 23. Ren Y, Tang J, Mok MY, Chan AW, Wu A, Lau CS. Increased apoptotic neutrophils and macrophages and impaired macrophage phagocytic clearance of apoptotic neutrophils in systemic lupus erythematosus. Arthritis Rheum **2003**; 48:2888–97.

- 24. Potter PK, Cores□Hernandez J, Quartier P, Botto M, Walport MJ. Lupus□prone mice have an abnormal response to thioglycolate and an impaired clearance of apoptotic cells. J Immunol **2003**; 170:3223–32.

- 25. Koh JS, Wang Z, Levine JS. Cytokine dysregulation induced by apoptotic cells is a shared characteristic of murine lupus. J Immunol **2000**; 165:4190–201.

- 26. Welliver TP, Garofalo RP, Hosakote Y, et al. Severe human lower respiratory tract illness caused by respiratory syncytial virus and influenza virus is characterized by the absence of pulmonary cytotoxic lymphocyte responses. J Infect Dis **2007**; 195:1126–36.

- 27. Thepen T, Van Rooijen N, Kraal G. Alveolar macrophage elimination in vivo is associated with an increase in pulmonary immune response in mice. J Exp Med **1989**; 170:499–509.

- 28. Gregoriadis G. Overview of liposomes. J Antimicrob Chemother **1991**; 28:39–48.

- 29. Santiago‐Raber ML, Baccala R, Haraldsson KM, et al. Type‐I interferon receptor deficiency reduces lupus‐like disease in NZB mice. J Exp Med **2003**; 197:777–88.

- 30. Samuel CE. Antiviral actions of interferons. Clin Microbiol Rev **2001**; 14:778–809.

- 31. Koszewski BJ, Emerick CW, Dicus DR. Studies of phagocytic activity of lymphocytes. III. Phagocytosis of intravenous India ink in human subjects. Blood **1957**; 12:559–66.

- 32. Oehen S, Odermatt B, Karrer U, Hengartner H, Zinkernagel R, López‐Macías C. Marginal zone macrophages and immune responses against viruses. J Immunol **2002**; 169:1453–58.

- 33. Ciavarra RP, Taylor L, Greene AR, et al. Impact of macrophage and dendritic cell subset elimination on antiviral immunity, viral clearance and production of type 1 interferon. Virology **2005**; 342:177–89.

- 34. Seiler P, Aichele P, Odermatt B, Hengarner H, Zinkernagel RM, Schwendener RA. Crucial role of marginal zone macrophages and marginal zone metallophils in the clearance of lymphocytic choriomeningitis virus infection. Eur J Immunol **1997**; 27:2626–33.

- 35. Londhe VA, Belperio JA, Keane MP, Burdick MD, Xue YY, Strieter RM. CXCR2/CXCR2 ligand biological axis impairs alveologenesis during dsRNA‐induced lung inflammation in mice. Pediatr Res **2005**; 58:919–26.

- 36. Kitamura Y, Hashimoto S, Mizuta N, et al. Fas/FasL‐dependent apoptosis of alveolar cells after lipopolysaccharide‐induced lung injury in mice. Am J Respir Crit Care Med **2001**; 163:762–9.

- 37. Laderach D, Bach JF, Koutouzov S. Nucleosomes inhibit phagocytosis of apoptotic thymocytes by peritoneal macrophages from $MRL^{+/+}$ lupus□prone mice. J Leukoc Biol **1998**; 64:774–80.

- 38. Haslett C. Granulocyte apoptosis and its role in the resolution and control of lung inflammation. Am J Respir Crit Care Med **1999**; 160:S5–11.

- 39. Vandivier RW, Fadok VA, Hoffmann PR, et al. Elastase□mediated phosphatidylserine receptor cleavage impairs apoptotic cell clearance in cystic fibrosis and bronchiectasis. J Clin Invest **2002**; 109:661–70.

- 40. Tyner JW, Uchida O, Kajiwara N, et al. CCL5□CCR5 interaction provides antiapoptotic signals for macrophage survival during viral infection. Nat Med **2005**; 11:1180–7.

- 41. Maródi L, Káposzta R, Campbell DE, Polin RA, Csongor J, Johnston RB Jr. Candidacidal mechanisms in the human neonate: impaired IFN□γ activation of macrophages in newborn infants. J Immunol **1994**; 153:5643–9.

- 42. Peters AM, Bertram P, Gahr M, Speer CP. Reduced secretion of interleukin□1 and tumor necrosis factor□α by neonatal monocytes. Biol Neonate **1993**; 63:157–62.

- 43. Stiehm ER, Sztein MB, Steeg PS, et al. Deficient DR antigen expression on human cord blood monocytes: reversal with lymphokines. Clin Immunol Immunopathol **1984**; 30:430–6.

- 44. Kurland G, Cheung AT, Miller ME, Ayin SA, Cho MM, Ford EW. The ontogeny of pulmonary defenses: alveolar macrophage function in neonatal and juvenile rhesus monkeys. Pediatr Res **1988**; 23:293–7.

- 45. Bakker JM, Broug□Holub E, Kroes H, van Rees EP, Kraal G, van Iwaarden JF. Functional immaturity of rat alveolar macrophages during postnatal development. Immunol **1998**; 94:304–9.

- 46. Nerurkar LS, Zeligs BJ, Bellanti JA. Maturation of the rabbit alveolar macrophage during animal development. II. Biochemical and enzymatic studies. Pediatr Res **1977**; 11:1202–11.

- 47. Zeligs BJ, Nerurkar LS, Bellanti JA. Maturation of the rabbit alveolar macrophage during animal development: phagocytic and bactericidal functions. Pediatr Res **1977**; 11:1208–11.

- 48. Tal G, Mandelberg A, Dalal I, et al. Association between common Toll□like receptor 4 mutations and severe respiratory syncytial virus disease. J Infect Dis **2004**; 189:2057–63.

- 49. Lahti M, Lofgren J, Marttila R, et al. Surfactant protein D gene polymorphism associated with severe respiratory syncytial virus infection. Pediatr Res **2002**; 51:696–9.

- 50. Hull J, Rowlands K, Lockhart E, Moore C, Sharland M, Kwiatkowski D. Variants of the chemokine receptor CCR5 are associated with severe bronchiolitis caused by respiratory syncytial virus. J Infect Dis **2003**; 188:904–7.

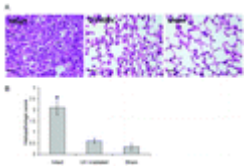

Figure B1. Validation of respiratory syncytial virus (RSV) strain A2 (RSVA2) stock in vivo. Six□week□old animals had light anesthesia induced by isoflurane administration. Three groups of mice (5–7 mice/group) received 100 mL of inocula of intact RSVA2 (10^6 pfu/dose) stock, the same viral stock that had been inactivated by ultraviolet irradiation for 30 min before inoculation, or saline vehicle control. Mice were permitted to inhale inoculum and then were placed in microisolator cages to recover from anesthesia. The experiment was terminated on day 6 after infection, and harvested lung tissue specimens were inflated with formalin. *A*, Representative micrographs of

hematoxylin–eosin (HE)–stained tissue obtained from each challenge group. The bar denotes 15 μm. *B,* A histopathologist who was blinded to the study groups analyzed HE–stained lung tissue specimens (from 5–7 mice/group). A score was assigned on a scale from 0 (denoting healthy tissue) to 3 (denoting highly inflamed and occluded tissue). The mean score (±SE) for each group is shown. *$P \leq .05$.

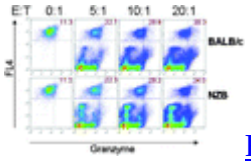

Figure B2. (76 KB)

Figure B2. Cell-mediated cytotoxicity assay. Cells obtained by bronchoalveolar lavage (BAL) on day 6 after infection were tested for cytotoxic activity. In brief, a respiratory syncytial virus (RSV)–permissive kidney cell line derived from the New Zealand black (NZB) mouse strain (NZBK; provided by Jay Levy, University of California, San Francisco, San Francisco) was double-labeled using a proprietary fluorescent dye and a granzyme B substrate that yields a fluorescent product when cleaved (both were purchased from OncoImmunin). Labeled cells were then infected with RSV strain A2 at an MOI of 10. Twenty-four h after in vitro infection, BAL-acquired lymphocytes were counted and added to the culture at an effector:target (E:T) ratio ranging from 0:1 to 20:1. After 2 h, conversion of the granzyme B substrate to its fluorescent product was assessed by flow cytometry. Cytolytic activity was expressed as the percentage of double-positive cells. Data representative of duplicate experiments are shown.

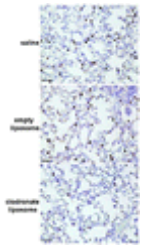

Figure B3. Depletion of alveolar macrophages in vivo by liposomes formulated with saline buffer with clodronate (hereafter referred to as “clodronate liposomes”). Six-week-old BALB/c mice had light anesthesia induced by administration of isoflurane. Three groups of mice (5–7 mice/group) were inoculated via the intranasal route with a 50-μL preparation of saline *(top),* empty liposomes in saline buffer *(middle),* or clodronate liposomes *(bottom).* The experiment was terminated 48 h later, and harvested lung tissue was inflated with formalin. Alveolar macrophages were identified by immunohistochemical analysis performed using an antibody reactive with galectin-3. Representative micrographs are shown. The bar denotes 30 μm.

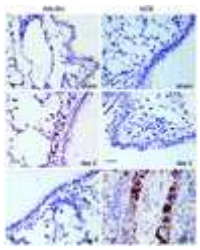

Figure B4. Detection of interferon‐inducible myxovirus resistance gene (Mx) proteins by immunohistochemical analysis (IHCA). IHCA was performed using polyclonal antibodies detecting Mx protein antigens (Chemicon) in lung tissue specimens obtained from BALB/c mice *(left)* or New Zealand black (NZB) mice *(right).* Tissue specimens sham infected with respiratory syncytial virus (RSV) *(top panels);* tissue specimens on day 2 *(middle panels)* and day 6 *(bottom panels)* after RSV infection. The bar denotes 15 μm.

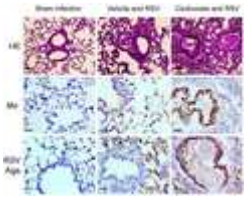

Figure B5. Depletion of lung macrophages and enhanced detection of respiratory syncytial virus (RSV) antigens (Ags) and interferon‐inducible myxovirus resistance gene (Mx) protein. Six‐week‐old BALB/c mice had light anesthesia induced by administration of isoflurane. Three groups of mice (7 mice/group) were inoculated via the intranasal route with 50 μL of saline or an equal volume of liposomes formulated with clodronate in saline. Two days later, each group was inoculated with 10^6 pfu of RSV strain A2 stock or vehicle control. The experiment was terminated on day 6 after infection. Lung tissue specimens were inflated with formalin, embedded in paraffin, and sectioned. Hematoxylin‐eosin (HE) staining was performed to assess general histopathologic assessment, and Mx and RSV antigens were detected by immunohistochemical analysis (IHCA). Representative micrographs are shown. The bar denotes 30 μm (for HE staining) or 15 μm (for Mx and RSV IHCA).

Table C1. Comparison of immune mediators and virus recovery in BALB/c and New Zealand black (NZB) mice.

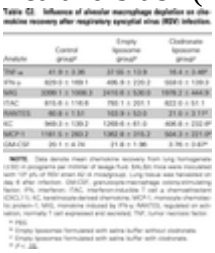

Table C2. Influence of alveolar macrophage depletion on chemokine recovery after respiratory syncytial virus (RSV) infection.

- Potential conflicts of interest: J.L.R., Y.A.B., T.D., T.B., E.B., E.K., A.K., L.M., J.S., P.A.K., A.H., and A.J.C. are employees of MedImmune, a for‐profit biotechnology company that develops monoclonal antibodies, including anti‐interferon and anti–respiratory syncytial virus F protein, for therapeutic use. T.W., L.A., L.V., and R.C.W. report no relevant conflicts.

Presented in part: 6th International Respiratory Syncytial Virus Symposium, Marco Island, Florida, 27 October 2007 (session 1, abstract 005).

Financial support: MedImmune (Gaithersburg, Maryland).

- Present affiliation: Department of Pulmonary and Critical Care Medicine, University of Michigan, Ann Arbor, Michigan.